Article

Monolayer Sc$_2$CF$_2$ as a Potential Selective and Sensitive NO$_2$ Sensor: Insight from First-Principles Calculations

Kai Cheng, Mengxia Wang, Sihao Wang, Nanshu Liu, Jinke Xu, Han Wang,* and Yan Su*

Read Online

ACCESS | Metrics & More | Article Recommendations | Supporting Information

ABSTRACT: Two-dimensional materials with excellent surface−volume ratios and massive reaction sites recently have been receiving attention for gas sensing. With first-principles calculations, we explored the performance of monolayer Sc$_2$CF$_2$ as a gas sensor. We investigated how molecule adsorption affects its electronic structure and optical properties. It is found that a large charge transfer quantity happens between Sc$_2$CF$_2$ and NO$_2$, which results from the fact that the lowest unoccupied molecular orbital (LUMO) of NO$_2$ is below the valence band maximum (VBM) of Sc$_2$CF$_2$. Moreover, the MD simulation shows that NO$_2$ can adsorb on the Sc$_2$CF$_2$ surface stably at room temperature. We explored the effect of biaxial strain on the adsorption energy and charge transfer quantity of each system, and the results show that the biaxial strain can enhance both the adsorption energy and charge transfer quantity of the NO$_2$ system and thus can improve the sensitivity of Sc$_2$CF$_2$ in detecting the NO$_2$ molecule. Furthermore, we investigated the adsorption behavior and charge transfer of polar polyatomic molecules at the Sc$_2$CF$_2$ surface with h-BN as a substrate, and the results demonstrate that the h-BN substrate can hardly modify the main results. Our result predicts that Sc$_2$CF$_2$ can be a promising selective and sensitive sensor to detect the NO$_2$ molecule, and could also give a theoretical guide for other terminated MXenes used for gas sensors or detectors.
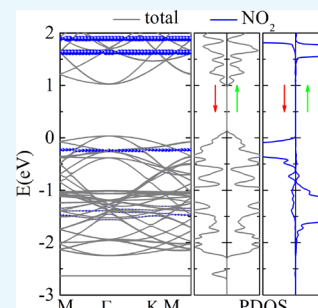
1. INTRODUCTION

Gas sensors and detectors play an important role in environmental protection and daily health safety applications. Because of the advantages of low costs, metal oxides have been explored widely; however, they require a high operating temperature.[1,2] With excellent surface−volume ratios and massive reaction sites, a large number of 2D materials including graphene,[3−5] h-BN,[6] phosphorene,[7−10] transition-metal chalcogenides,[11−13] and layered group III−VI semi-conductors[14−17] have been reported with superior performance for detecting gas.[18−21] Charge transfer happens when molecules are adsorbed on 2D materials, and the charge transfer between molecules and 2D materials will modify the electronic structures and/or resistance of sensing materials by varying degrees. A copious amount of charge transfer is required for high selectivity and sensitivity 2D sensing materials.

MXenes, including traditional metal carbides, nitrides, and carbon-nitrides with possible stoichiometric ratios of 2:1, 3:2, and 4:3, are a large family of 2D materials,[22−24] which are usually synthesized through chemical exfoliation from the MAX phase by etching the "A" atoms in acid solutions. Meanwhile, the intrinsic metallic surface of MXenes is usually passivated or terminated by a function group, and there consist four passivation models depending on function group adsorption sites on both sides.[25−27] With a natural layered structure, MXenes have been explored as high-performance electrode materials in lithium-ion batteries.[28−32] For instance, bare Ti$_3$C$_2$ shows excellent theoretical capacity and low Li-ion

diffusing barrier,[30] and the rate performance of terminated Ti$_3$C$_2$ can be greatly enhanced after intercalation.[31,32] MXenes also find potential applications in other energy storage aspects, like supercapacitors,[33−35] Li-S batteries,[36] and multivalent-ion batteries.[37−39] Owing to their intrinsic metallic property, MXenes flakes, which have low average resistivity and high electron mobility, also have been reported to be used as a conductive channel in field-effect transistors, which may construct an Ohmic contact.[40,41] Besides, low-thickness Ti$_2$CX$_2$ films with a transmittance of about 90% have been explored as transparent conductive electrodes.[42−44] It has also been reported that active sites for water redox exist in MXenes, which also show suitable Gibbs free energy for hydrogen adsorption and are electro-catalyst or photo-catalyst candidates for water splitting.[45−47] MXenes have found promising application in various fields.

Besides, MXenes also have been explored as sensing materials for sensors or detectors. In terms of theoretical calculations, MXenes have been widely explored for gas sensing. Density functional theory (DFT) calculations demonstrated that bare MXenes are reactive, where molecules'
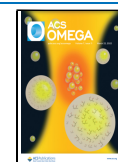
dissociative adsorption happens at most surfaces, and the selectivity is enhanced upon surface functionalization.[48] DFT calculations along with non-equilibrium Green's function (NEGF) method simulation predicted that O-terminated Ti_2C can detect NH_3 sensitively with a strong binding energy. A dramatic change of the $I-V$ curve after NH_3 adsorption determines the selectivity of O-terminated Ti_2C.[49] In addition, applied strain can increase the binding energy and improve the sensitivity, while releasing the strain or injecting an electron into MXenes will weaken the strength and achieve reusability of sensing materials.[49,50] Similarly, it has been reported that SO_2 can be detected by Sc_2CO_2 with suitable adsorption energy. Moreover, biaxial strain and external vertical electric field can help SO_2 desorption from Sc_2CO_2.[51] In terms of experiments, Wang et al. have reported that stacked $Ti_3C_2T_X$ molecular sieving membranes exhibit excellent H_2 permeability, which mainly benefit from the sub-nanometer interlayer spacing between the neighboring MXene nanosheets.[52] Stanciu et al. designed a nanohybrid structure with MXene ($Ti_3C_2T_X$) and transition metal dichalcogenide (WSe_2), which can adsorb oxygen species (O_2^- and O^-) in air and exhibits good flexibility for O-containing volatile organic compounds with low noise and fast response/recovery speed.[53]

To our best knowledge, MXenes are potential candidates for gas sensors. Here, we performed DFT calculations to explore the adsorption of 11 common molecules on F-terminated Sc_2C (Sc_2CF_2) and their charge transfer, which have not been studied yet. We investigated how molecule adsorption affects their electronic structure and optical properties. It is found that the largest charge transfer quantity happens between Sc_2CF_2 and NO_2, which is because the lowest unoccupied molecular orbital (LUMO) of NO_2 is below the valence band maximum (VBM) of Sc_2CF_2, although the adsorption energy is not very large. The adsorption stability and sensitivity of Sc_2CF_2 sensing NO_2 are demonstrated through molecular dynamics simulation with an NVT ensemble, and applying biaxial strain is claimed to be a promising method for enhancing the sensitivity and selectivity. Besides, h-BN as a substrate can hardly modify the adsorption energy and charge transfer at the polar polyatomic molecules' adsorption system and is a promising substrate. These results indicate that F-terminated Sc_2C is a good candidate for a NO_2 gas sensor, and give a theoretical guide for other terminated MXenes used for gas sensors or detectors.

2. RESULTS AND DISCUSSION

To simulate the Sc_2CF_2 monolayer exposed in air, we place 11 common molecules on the surface of Sc_2CF_2, and several adsorption configurations, i.e., top, bridge, and hollow sites of the three top F atoms, as well as the vertical and parallel orientation of each molecule, are considered. To characterize the interaction strength between the molecule and the 2D sheet, we define the adsorption energy (E_{ads}) as $E_{ads} = E_{tot} - E_{2D} - E_{gas}$, where E_{tot} and E_{2D} are the energies of the monolayer Sc_2CF_2 with and without adsorption of a gas molecule, respectively; E_{gas} is the energy of a gas molecule in a cubic lattice with a lattice constant of 15 Å. The most stable configurations and E_{ads} for each molecule system are shown and listed in Figure 1 and Table 1. The homo-nuclear diatomic molecules, like H_2, O_2, and N_2, will stay parallel to the substrate, and the weakest interaction with E_{ads} ranging from −0.07 to −0.09 eV per molecule is found in these cases. The polar hetero-nuclear diatomic molecules, like NO and CO, also remain parallel with Sc_2CF_2, and the E_{ads} is also small;
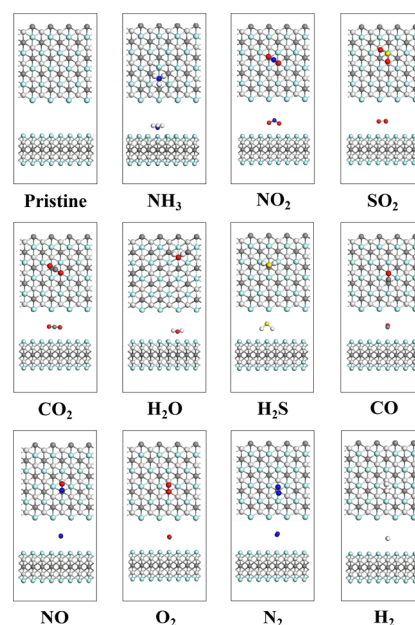

Figure 1. Most stable adsorption configurations for 11 molecules (light gray balls for Sc atoms, gray for C, light blue for F, white for H, dark blue for N, red for O, and yellow for S). The upper panels are the top view, and the lower panels are the side view of each molecule.

Table 1. Adsorption Energy per Unit Cell (E_{ads}), Vertical Distances along z Direction (D_Z), Average Distance to the Parent Nanosheet (D), Charge Transfer (CT), Bandgaps (E_g), Electron (m_e^*) and Hole (m_h^*) Effective Mass, and Work Function of Molecules Adsorbed on the Surface of Sc_2CF_2 [a]

	E_{ads} (eV)	D_Z (Å)	D (Å)	CT $(10^{-3}$ $e)$	E_g (eV)	m_e^* (m_0)	m_h^* (m_0)	W_F (eV)
bare					1.02	0.98	2.32	4.71
NH_3	−0.39	1.54	2.53	−83.5	0.99	0.71	2.03	4.57
NO_2	−0.21	2.33	2.93	100.3	0.99	0.90	2.13	5.17
SO_2	−0.21	2.59	3.02	8.9	1.00	0.69	1.93	4.72
H_2O	−0.20	1.81	2.24	−19.7	0.99	0.68	1.96	4.99
H_2S	−0.18	2.28	2.38	−4.7	1.00	0.89	1.91	4.99
CO_2	−0.16	2.57	3.04	4.6	1.01	0.90	2.18	4.73
CO	−0.14	2.66	3.13	−2.7	0.99	0.79	1.97	4.86
NO	−0.13	2.92	3.38	1.2	1.00	0.90	2.13	4.44
O_2	−0.09	2.64	3.21	−1.7	0.99	0.81	1.92	4.99
H_2	−0.07	2.28	2.64	−3.9	1.00	0.68	1.96	4.84
N_2	−0.09	3.19	3.58	0.5	1.00	0.93	2.08	4.75

[a]Negative CT values represent electron transfer from molecules to the Sc_2CF_2 sheet.

however, it is a little stronger than that of the homo-nuclear diatomic molecule ($E_{ads} = -0.13$ and -0.14 eV for NO and CO, respectively), which is due to the strong electronegativity of the surface F atoms of the substrate. The CO_2 molecule has no polarity and contacts weakly with Sc_2CF_2. For polar polyatomic molecules (H_2S, H_2O, SO_2, NO_2, and NH_3), the adsorption is much stronger. The E_{ads} of H_2O and H_2S is −0.20 and − 0.18 eV per molecule, respectively, and the H in both cases will favor staying at the top of F, while the O in H_2O tends to stay at the top of Sc and S prefers the top of C. The NO_2 is more likely to stand vertically on the substrate, while SO_2 prefers to lie parallel on the surface. In the case of
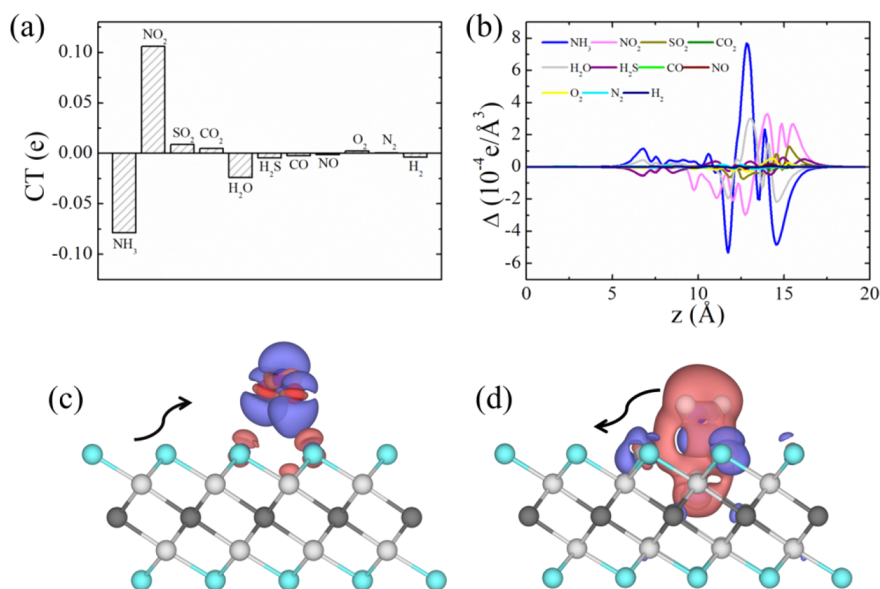
Figure 2. (a) Charge transfer from molecules to Sc_2CF_2 (calculated from Bader charge analysis). (b) Planar average charge density difference projected along the z direction. Spatial charge density differences of (c) NO_2 and (d) NH_3 adsorbed on Sc_2CF_2 with an isosurface of 0.05 e/Bohr^3. The purple and magenta regions indicate electron accumulation and depletion, respectively. The arrow specifies the direction of electron transfer.

SO_2 and NO_2, the O atoms favor to stay at the top or bridge of Sc. Actually, the O atom from different molecules shares the same character in all cases. The NH_3 shows the strongest adsorption behavior with E_{ads} of −0.39 eV and vertical distance along the z direction of 1.54 Å. As shown in Figure 1, the NH_3 molecule favors to stack parallel on the 2D sheets, with the N atom staying at the top of Sc and three H atoms sharing symmetrically three hollow sites of neighboring F atoms. The coupling between the nanosheet and NH_3 will change the bond angles of H−N−H from 106.57 to 107.27°; meanwhile, the F atoms of nanosheets near the adsorption site move slightly away from the original position because the N partially shares the lone pair of electrons with Sc.

Once the molecule is adsorbed on the surface, the electronic structures of whole systems change and charge will redistribute between the molecule and nanosheet. Bader charge calculations are performed to determine the electron on each single atom so that we can see the charge transfer quantity induced by the gas molecule adsorption. As shown in Table 1 and Figure 2a, small amount of charge transfer (0.0005−0.0046 e) has been found in diatomic molecules and non-polar cases (N_2, H_2, O_2, CO, NO, and CO_2), and more charge transfer can be found in polar polyatomic molecules. The H_2S, H_2O, and NH_3 act as electron donors and transfer 0.0047, 0.0197, and 0.0835 e to Sc_2CF_2, respectively, while SO_2 serves as an electron acceptor and obtains 0.0087 e from Sc_2CF_2. Especially, the largest charge transfer happens at the NO_2 system, and NO_2 takes 0.1003 electron from 2D materials, although the vertical distance between NO_2 and Sc_2CF_2 is larger than that of the NH_3 system. Furthermore, we calculated the charge density difference and projected it along the z direction as shown in Figure 2b. It can be seen that the polar polyatomic molecules' adsorption systems show obvious oscillation at the interface region, especially the NH_3, NO_2, and H_2O systems, which is consistent with the result from Bader analysis. To show the details, the spatial charge density difference for NO_2 and NH_3 adsorption on the Sc_2CF_2 surface is plotted in Figure 2c,d, respectively. In the case of NO_2, all atoms at NO_2 and even the

O atoms, which correspond with the three immediate neighboring positive peaks at about 13.5, 14, and 14.5 Å in Figure 2b, will accept electrons from the substrate and even from Sc atoms, which are located far away from the interface (see Figure 2c). The adsorption of NO_2 will induce a large interface dipole at the interface region, with electron accumulation at the NO_2 molecule side and electron depletion at the substrate side. As NH_3 attaches on Sc_2CF_2, electrons from the NH_3 molecule orbital, which are mainly from the three H atoms in Figure 2d and correspond with the large valley near 14 Å in Figure 2b, transfer into Sc_2CF_2 and mainly into F atoms at the interface (see Figure 2d). Meanwhile, the adsorption of NH_3 will induce a surface dipole at Sc_2CF_2, with electron accumulation near the surface of F atoms and electron depletion near Sc atoms at the subsurface. In the case of H_2O, H atoms still prefer to donate electrons, which correspond the valley near 14.5 Å, and O atoms still like to accept electrons, which correspond the peak near 13 Å in Figure 2b. In total, few electrons will transfer from H_2O into the substrate, which also produces a small surface dipole at the surface of Sc_2CF_2. According to the transferred charge quantity, we can see the selectivity of Sc_2CF_2 to detect the NO_2 molecule.

To explain the physical causes of charge transfer, we calculated the band structures and density of states (DOS) of the adsorption system and extracted individual contributions of the molecule and substrate. Figure 3 show the results for NH_3, SO_2, NO, and NO_2 adsorption systems. Several flat bands appear after adsorption, whose position has a close relationship with the alignment of frontier molecular orbitals of molecules and bands of pristine Sc_2CF_2. The isolated NH_3 molecule has a HOMO−LUMO gap of 5.4 eV from DFT calculation. Both the HOMO and LUMO of isolated NH_3 are far away from the VBM and conduction band minimum (CBM) of pristine Sc_2CF_2; thus, the flat bands of the NH_3 adsorption system stay away from the Fermi level. However, the shortest vertical distance between NH_3 and Sc_2CF_2 makes the strongest wave-function mixing or electronic state coupling, which induces the large peaks at the energy range from −2.5 to −0.3 eV at the
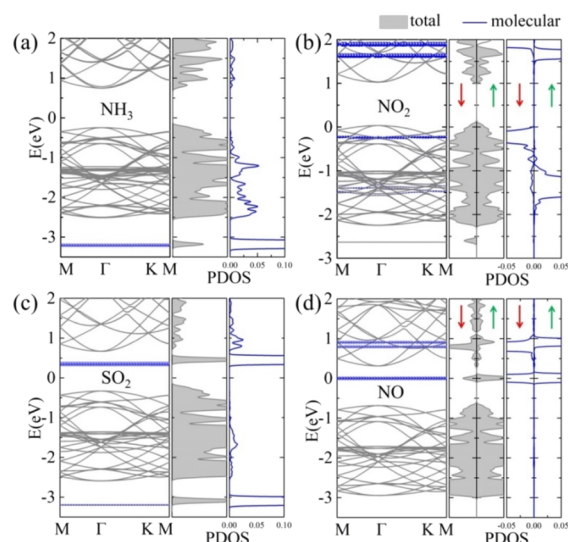
Figure 3. Band structures and projected DOS of (a) NH_3, (b) NO_2, (c) SO_2, and (d) NO adsorption systems. In the left panels, the gray lines are the band structure of the whole system, and the Fermi level is set as 0. The blue spheres correspond to the states with valid contribution from molecules, and the radii of spheres are proportional to the weight. In the middle and right panels, the dark gray lines filled with gray solid pattern are the total DOS of systems, and the blue lines are the PDOS of the molecules.

partial DOS plot in Figure 3a. The strongest wave-function coupling opens a charge transfer channel, which results in a large amount of charge transfer between NH_3 and Sc_2CF_2. For the SO_2 adsorption system, the LUMO of the molecule is located at the forbidden band region of Sc_2CF_2, while the HOMO is located at the deep valance band region as seen from Figure 3c. The vertical distance is longer than that of the NH_3 system; thus, there is less wave-function mixing, demonstrating much less charge transfer. For open-cell NO, the half-filled doubly degenerated antibonding HOMO (2π orbital with spin-up), together with its spin-split partner unoccupied LUMO (2π orbital with spin-down), becomes non-degenerated because of the symmetry breaking after contacting with the substrate. We named the non-degenerated HOMO orbital at the higher energy as $HOMO_1$ and the other as $HOMO_2$, and the non-degenerated LUMO at the lower energy level as $LUMO_1$ and the other as $LUMO_2$ for convenience. The two HOMO orbitals are mid-gap states after adsorption, and the initial empty $HOMO_1$ stays above the Fermi level. As a polar hetero-nuclear diatomic molecule, the E_{ads} of NO is pretty small, which means weak wave-function mixing and is consistent with the small amount of charge transfer from the Bader calculation. It should be noticed that $HOMO_1$ is still contributed from electrons of spin-up while $HOMO_2$ is contributed from electrons of spin-down, which is totally different from the isolated NO molecule, indicating the large decrease of magnetic moment after adsorption (from 1 to 0.06 μB). The case of the NO_2 adsorption system is very different from the three cases above, where the LUMO ($6a_1$ molecule arbitral with spin-down) of NO_2 is located below the VBM of Sc_2CF_2; thus, a large amount charge will transfer from the substrate to NO_2 to fill the LUMO orbital of NO_2. The valance band at some K points of the NO_2 adsorption system is partially occupied or even unoccupied, and metal behaviors indicate a total change of the electronic structure after NO_2

adsorption. Besides, the charge transfer between the Sc_2CF_2 substrate and paramagnetic NO_2 also reduces the magnetic moment of the whole system by 0.91 μB.

The rest electronic structure information of the molecules is summarized in Table 1. The bandgap after adsorption does not change much according to Table 1; however, the effective mass changes because of the wave-function mixing. For instance, the orbital of SO_2 couples more strongly with the conduction band of Sc_2CF_2 (Figure 3c), and the effective mass of the hole changes by 0.39 m_0. Besides, the effective mass of both electrons and holes decreases for each adsorption case, which means the increasing of carrier mobility. It is worth noting that the work function after NO_2 adsorption increases by 0.46 eV, which is even larger than what has been reported for graphene.[58]

Furthermore, we explored the optical properties for each system, which may be useful in optical chemistry gas sensors. The imaginary part of dielectric function and adsorption coefficient are plotted at Figure 4. At the range of visible light,
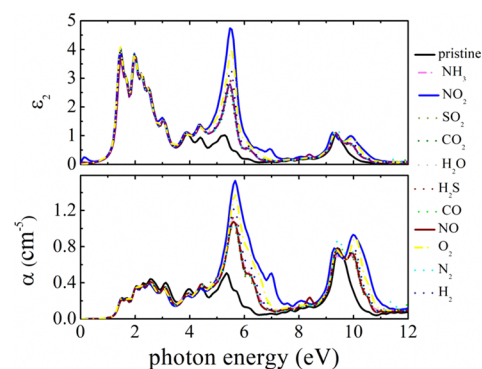

Figure 4. Imaginary part of dielectric function for the polarization vector perpendicular to the surface and absorption coefficient of Sc_2CF_2 systems with and without molecules adsorbed on the surface.

little change can be found except for a slight intensity decrease and negligible red-shift of the main peaks. However, a clear difference occurs at the ultraviolet range. There are two major absorption peaks (located at 5.3 and 9.4 eV) at the ultraviolet range for pristine Sc_2CF_2. The intensity of the peak located around 5.3 eV is greatly enhanced after molecules adsorbed at each adsorption system, especially for the case of NO_2. Meanwhile, an evident blue-shift happens, and the corresponding peak at the NO_2 system moves into around 5.7 eV. The other peak around 9.4 eV changes little except for a slight red-shift. More importantly, the adsorption of each molecule induces a new peak around 9.9 eV, and the NO_2 system shows the strongest absorption intensity here. It should also be noted that the adsorption of NO_2 induces two additional peaks, which are located around 0.1 and 7.0 eV, respectively. The peak of 0.1 eV has a direct relationship with the partial occupied or unoccupied states near VBM. The quite different optical properties after NO_2 adsorption indicate the potential application of Sc_2CF_2 as a NO_2 optical chemistry sensor.

In the aspect of electronic and optical structures, we have found the selectivity of Sc_2CF_2 to detect NO_2. To explore the adsorption thermal stability of NO_2 at the Sc_2CF_2 surface, we performed *ab initio* molecular dynamics (MD) simulations with an NVT ensemble at a temperature of 300 K for about 11 ps. The time evolution of vertical distances between each atom of NO_2 and the top F atom layer of Sc_2CF_2 is summarized in

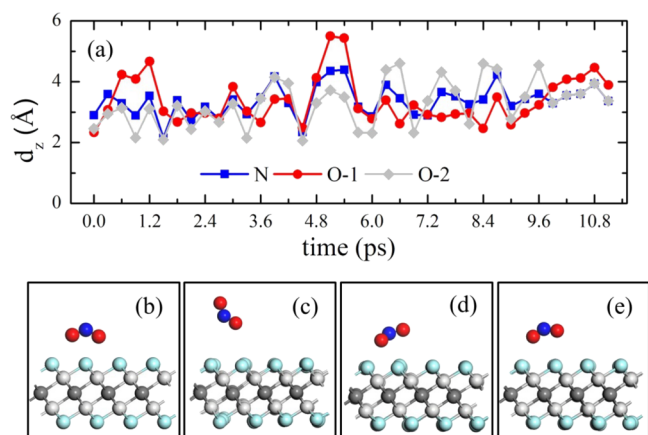Figure 5a, in which two O atoms of NO_2 are labeled as O-1 and O-2 to distinguish them. During the MD process, the

Figure 5. (a) Evolution of vertical distances for each atom of NO_2 with the top F layer of Sc_2CF_2 at first-principles molecule dynamics simulations. Snapshot of the NO_2 adsorption system at time of (b) 0 ps, (c) 5.1 ps, (d) 6.9 ps, and (e) 11.1 ps, respectively.

Sc_2CF_2 layer prefers to contact with O atoms (O-1 or O-2) of the NO_2 molecule, and the smallest vertical distance is maintained at the range of 2−4 Å. Compared with the initial structure, the system changes most at time 5.1 ps, when the vertical distance of N, O-1, and O-2 reaches up to 4.35, 5.49, and 3.72 Å, respectively. However, the NO_2 molecule bounces back rapidly, and the vertical distance of N, O-1, and O-2 becomes 3.18, 3.11, and 2.33 Å at time 5.7 ps, respectively. From the MD simulation, it can be seen that the NO_2 molecule only vibrates around its equilibrium positions, revealing that NO_2 can adsorb on the 2D surface stably at room temperature.

Strain modulation is reported as an effective method to improve the performance of 2D materials. A uniaxial strain can be applied through bending, rolling up, and elongation in experiments, and a homogeneous biaxial strain can also been applied into 2D materials through a substrate that has a different thermal expansion coefficient with 2D materials or a substrate that is a piezoelectric material.[59−62] Most 2D materials have a fracture strain value over or about 10%,[63−66] and we enlarge the lattice of the Sc_2CF_2 substrate by 1−9% to explore the strain effect on adsorption energy and sensitivity. As shown in Figure 6, the adsorption of NO_2, NH_3, and H_2O changes the most, and other systems are not sensitive to biaxial strain. As biaxial strain increases, the E_{ads}'s of NH_3 and H_2O increase monotonously. For the strained NO_2 system, the E_{ads}'s start to increase with strain up to 4%, and the increase rate is much larger than that of both NH_3 and H_2O. As we all know, the adsorption energy can be influenced by the polarity of the molecules at gas molecule adsorption systems, and the polar molecule usually shows a larger adsorption energy than the nonpolar molecules as we discussed above. Besides, the atoms at the surface and subsurface should also have an effect on the adsorption energy. For instance, the well-saturated surfaces usually prefer to adsorb no molecule or adsorb molecules weakly, while the surfaces with unsaturated bonds usually like to adsorb molecules more strongly. When biaxial strain is applied, the symmetry of Sc_2CF_2 is destroyed to some degree and becomes not so well-saturated, and the adsorption of molecules will be enhanced. Thus, strain modulation is an effective method to improve the adsorption energy and
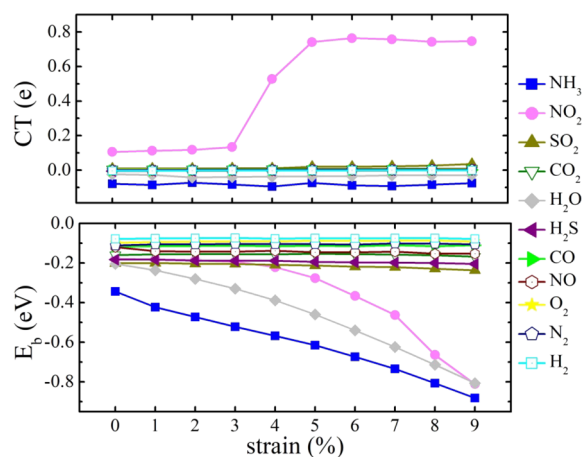

Figure 6. The transferred charge and adsorption energy of each system when applied with biaxial strain from 1 to 9%.

sensitivity. We also explored the effect of biaxial strain on charge transfer, as shown in Figure 6. Different from the adsorption energy, the charge transfer is not sensitive to strain even for the NO_2 system with strain less than 3%, and it seems that the charge transfer has no direct relationship with the adsorption energy for each molecule adsorption system. The charge transfer is on one hand affected by the distance between them, and a smaller distance usually results in a large charge transfer. On the other hand, the electron state coupling will also make a great contribution, and the molecular orbitals of gas molecules, which have a similar energy level with the electron states of Sc_2CF_2, are the charge transfer channel. The biaxial strain can hardly change the molecular orbitals; thus, we can see that the charge transfer is not sensitive to biaxial strain for most systems. However, in the case of NO_2 adsorption, the LUMO of NO_2 is very close with the VBM of Sc_2CF_2. To demonstrate the effect of strain on charge transfer in the case of NO_2, we further explored the band structures of the NO_2 adsorption system with a biaxial strain of 1, 4, and 7%, as shown in Figure S2 of the Supporting Information. It can be seen that the band structures, mainly the band (molecule orbital) alignment, are modified much with biaxial strain. When there is no strain, the alignment is type III, with the LUMO of NO_2 below the VBM of Sc_2CF_2. The alignment becomes type II with the LUMO of NO_2 moving up above the VBM of Sc_2CF_2 once strain is 1% at Sc_2CF_2. The band structure of 4% biaxial strain is similar with that of 1%; however, the band structure is altered much when strain continues increasing. When strain is 7%, the alignment reverts into type III with the LUMO of NO_2 below the VBM of Sc_2CF_2, which is due to the large biaxial strain breaking the lattice symmetry of the Sc_2CF_2 substrate and thus modifying the electronic structure of Sc_2CF_2 near the band edge. In total, biaxial strain can enhance both the adsorption energy and charge transfer for the NO_2 adsorption system and is an effective method to improve the sensitivity and selectivity of Sc_2CF_2 to detect the NO_2 molecule.

Under real situations, 2D materials are typically supported by a substrate, which influences their electronic properties as well as the adsorption of molecules on their surface. SiO_2 is a common substrate for 2D material applications in electronics or optoelectronics, which is cheap, flat, and chemically inert. However, SiO_2 really can give a great effect on the properties of 2D materials, and some researchers try to use h-BN as a
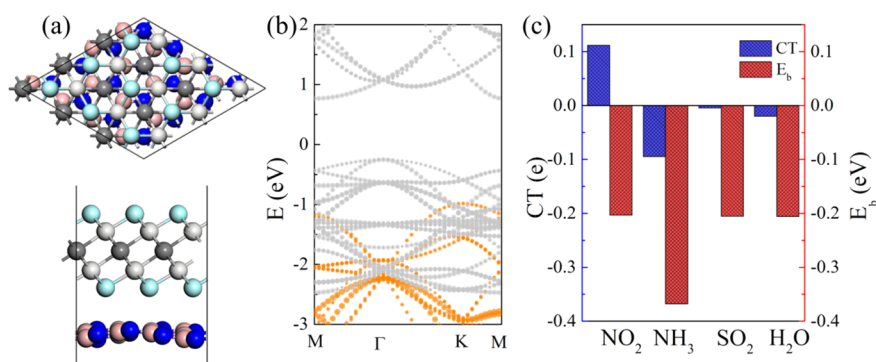
Figure 7. (a) Atomic structures of the Sc_2CF_2/h-BN supercell: top view (upper) and side view (lower); pink balls are B atoms, and blue balls are N atoms. (b) Projected band structure of the Sc_2CF_2/h-BN supercell: gray parts are the contribution from Sc_2CF_2, and orange parts are the contribution from h-BN. (c) Charge transfer and adsorption energy of NO_2, NH_3, SO_2, and H_2O adsorbed on the surface of Sc_2CF_2 with h-BN as a substrate.

substrate or use h-BN as a substrate on top of SiO_2/Si, which will reduce the effect of SiO_2.[67,68] Here, we considered h-BN as a substrate for Sc_2CF_2 and explored the effect of h-BN. The lattice constant of h-BN after optimization is 2.41 Å. We used a 3×3 Sc_2CF_2 supercell to match with 4×4 h-BN vertically as shown in Figure 7a, and the mismatch is about 1.43%. After optimization, Sc_2CF_2 is still flat and there exists some buckling in h-BN, which however still maintains the honeycomb structure from the top view. It can be seen from the projected band structure of Sc_2CF_2/h-BN heterostructures in Figure 7b that the electronic structure of Sc_2CF_2 can be hardly affected by the h-BN substrate, and a type III band alignment is found. Then we considered four polar polyatomic molecules, that is, NO_2, NH_3, SO_2, and H_2O, adsorbed at the surface of Sc_2CF_2/h-BN. The calculated E_{ads} and charge transfer from Bader charge analysis are also plotted in Figure 7c. Here, we used a 3×3 supercell, which is a little different from the model before and may have an effect on the value of E_{ads} and charge transfer. However, the trends of both the adsorption energy and charge transfer are not modulated. The NH_3 shows the largest adsorption energy, and the E_{ads} of NO_2, NH_3, and SO_2 is about 0.21 eV. The largest charge transfer occurs in the case of NO_2, and NH_3 shows more charge transfer than both H_2O and SO_2. Furthermore, we calculated the projected band structures for four adsorption systems with the h-BN substrate as shown in Figure S3 in the Supporting Information. In total, the relative position of the molecular orbital with bands of Sc_2CF_2 changes little, and the LUMO of NO_2 is still partially occupied after absorption, which induces a large amount of charge transfer. These results demonstrate that the h-BN substrate can hardly affect the main results from calculations with a free-standing Sc_2CF_2. Also note that we considered a pristine Sc_2CF_2 layer here and the charge transfer will always enhance the carrier density. However, the defect is inevitable in experiments. If the presence of defects makes Sc_2CF_2 show n-type/p-type conductivity, the carrier density and conductivity do not depend on the charge transfer only. The electron/hole transfer into Sc_2CF_2 will improve/decrease the n-type conductivity, and the hole/electron transfer into Sc_2CF_2 will improve/decrease the p-type conductivity. Thus, the predicted obvious selectivity and sensitivity of Sc_2CF_2 to detect NO_2 still need to be confirmed by future experiments.

3. CONCLUSIONS

In summary, we have studied several molecules' adsorption behaviors on Sc_2CF_2 and explored the charge transfer between molecules and Sc_2CF_2. Using first-principles calculations, we have investigated the structural, electronic, and optical properties of adsorption systems. The results show that the largest charge transfer quantity happens between NO_2 and Sc_2CF_2, and optical properties of the system are modified by the NO_2 molecule obviously, both of which are due to the special electronic structure, where the LUMO of NO_2 is below the VBM of Sc_2CF_2. Thus, Sc_2CF_2 can detect the NO_2 molecule selectively. Moreover, the MD simulation shows that NO_2 can adsorb on the Sc_2CF_2 surface stably at room temperature. Besides, we explored the effect of biaxial strain on the E_{ads} and charge transfer quantity of each system, and the result shows that the biaxial strain can enhance both adsorption energy and charge transfer and improve the sensitivity of Sc_2CF_2 to detect the NO_2 molecule. Furthermore, we investigated how h-BN will affect the adsorption behavior and charge transfer, revealing that the h-BN is a potential substrate for Sc_2CF_2 sensors. Our result predicts that Sc_2CF_2 can be a promising selective and sensitive sensor to detect the NO_2 molecule.

4. COMPUTATIONAL DETAILS

All first-principles calculations were carried out using the Vienna Ab initio Simulation Package (VASP)[54] based on DFT with a plane-wave basis set. To treat the exchange−correlation interaction of electrons, we chose the Perdew−Burke−Ernzerhof (PBE) functional[55] within the generalized gradient approximation (GGA). The electron−ion interactions were described by the projector augmented wave (PAW) potentials.[56] The energy cutoff for the plane-wave basis was chosen as 600 eV, and the Brillouin zones (BZs) were sampled by k grids with a uniform spacing of $2\pi \times 0.02$ Å^{-1}. Convergence criteria of 10^{-4} eV for total energy and 0.01 eV/Å for force were adopted for self-consistent calculation and geometry optimization, respectively. We chose a 4×4 supercell to simulate the periodic structure of Sc_2CF_2 monolayers, and a vacuum spacing of 20 Å was added along the direction perpendicular to the 2D sheet (z direction) to avoid interaction between adjacent layers. To properly describe the van der Waals interaction between gas molecules and the Sc_2CF_2 sheet, we adopted the semi-empirical dispersion-corrected DFT-D3 scheme proposed by Grimme.[57] Spin

polarization was included for the systems adsorbed by paramagnetic molecules like NO, NO_2, and O_2. Dipole correction was added in the average potential calculation for the system adsorbed by polar molecules. Various initial configurations with different adsorption sites and molecule orientations of the gas molecules were considered here. The initial distance between the gas molecule and 2D nanosheet was chosen to be 2.0 Å.

ASSOCIATED CONTENT

Supporting Information

The Supporting Information is available free of charge at https://pubs.acs.org/doi/10.1021/acsomega.1c06027.

> DOS of free (a) NO and (b) NO_2 molecule, and inset is the charge density plot (Figure S1); band structures of NO_2 adsorption systems with biaxial strain (Figure S2); and projected band structure with (a) NO_2, (b) NH_3, (c) H_2O, and (d) SO_2 adsorbed at the Sc_2CF_2 surface with h-BN as a substrate. The blue parts are the contribution from the molecule, the gray parts are from Sc_2CF_2, and the orange parts are from h-BN (PDF)

AUTHOR INFORMATION

Corresponding Authors

Han Wang − *Department of Physics, Applied Physics, and Astronomy, Rensselaer Polytechnic Institute, Troy, New York 12180, United States; Chemical Sciences Division, Lawrence Berkeley National Laboratory, Berkeley, California 94720, United States;* ⊙ orcid.org/0000-0002-7476-6012; Email: wangh0606@gmail.com

Yan Su − *Key Laboratory of Materials Modification by Laser, Ion and Electron Beams (Dalian University of Technology), Ministry of Education, Dalian 116024, China;* ⊙ orcid.org/0000-0001-5669-9015; Email: su.yan@dlut.edu.cn

Authors

Kai Cheng − *School of Electronic Engineering, Xi'an University of Posts and Telecommunications, Xi'an 710121, China; Key Laboratory of Materials Modification by Laser, Ion and Electron Beams (Dalian University of Technology), Ministry of Education, Dalian 116024, China; Department of Physics, Applied Physics, and Astronomy, Rensselaer Polytechnic Institute, Troy, New York 12180, United States*

Mengxia Wang − *School of Electronic Engineering, Xi'an University of Posts and Telecommunications, Xi'an 710121, China*

Sihao Wang − *School of Electronic Engineering, Xi'an University of Posts and Telecommunications, Xi'an 710121, China*

Nanshu Liu − *Key Laboratory of Materials Modification by Laser, Ion and Electron Beams (Dalian University of Technology), Ministry of Education, Dalian 116024, China*

Jinke Xu − *School of Electronic Engineering, Xi'an University of Posts and Telecommunications, Xi'an 710121, China*

Complete contact information is available at:
https://pubs.acs.org/10.1021/acsomega.1c06027

Notes

The authors declare no competing financial interest.

ACKNOWLEDGMENTS

REFERENCES

(1) Kanazawa, E.; Sakai, G.; Shimanoe, K.; Kanmura, Y.; Teraoka, Y.; Miura, N.; Yamazoe, N. Metal oxide semiconductor N_2O sensor for medical use. *Sens. Actuators, B* **2001**, *77*, 72−77.

(2) Korotcenkov, G. Metal oxides for solid-state gas sensors: What determines our choice? *Mater. Sci. Eng., B* **2007**, *139*, 1−23.

(3) Leenaerts, O.; Partoens, B.; Peeters, F. M. Adsorption of H_2O, NH_3, CO, NO_2 and NO on graphene: A first-principles study. *Phys. Rev. B* **2008**, *77*, 125416.

(4) Schedin, F.; Geim, A. K.; Morozov, S. V.; Hill, E. W.; Blake, P.; Katsnelson, M. I.; Novoselov, K. S. Detection of individual gas molecules adsorbed on graphene. *Nat. Mater.* **2007**, *6*, 652−655.

(5) Wehling, T. O.; Novoselov, K. S.; Morozov, S. V.; Vdovin, E. E.; Katsnelson, M. I.; Geim, A. K.; Lichtenstein, A. I. Molecular Doping of Graphene. *Nano Lett.* **2008**, *8*, 173−177.

(6) Khan, A. F.; Brownson, D. A. C.; Randviir, E. P.; Smith, G. C.; Banks, C. E. 2D Hexagonal Boron Nitride (2D-*h*BN) Explored for the Electrochemical Sensing of Dopamine. *Anal. Chem.* **2016**, *88*, 9729−9737.

(7) Abbas, A. N.; Liu, B.; Chen, L.; Ma, Y.; Cong, S.; Aroonyadet, N.; Köpf, M.; Nilges, T.; Zhou, C. Black Phosphorus Gas Sensors. *ACS Nano* **2015**, *9*, 5618−5624.

(8) Shukla, V.; Wärnå, J.; Jena, N. K.; Grigoriev, A.; Ahuja, R. Toward the Realization of 2D Borophene Based Gas Sensor. *J. Phys. Chem. C* **2017**, *121*, 26869−26876.

(9) Cui, S.; Pu, H.; Wells, S. A.; Wen, Z.; Mao, S.; Chang, J.; Hersam, M. C.; Chen, J. Ultrahigh sensitivity and layer-dependent sensing performance of phosphorene-based gas sensors. *Nat. Commun.* **2015**, *6*, 8632.

(10) Kou, L.; Frauenheim, T.; Chen, C. Phosphorene as a Superior Gas Sensor: Selective Adsorption and Distinct I−V Response. *J. Phys. Chem. Lett.* **2014**, *5*, 2675−2681.

(11) Choi, W.; Choudhary, N.; Han, G. H.; Park, J.; Akinwande, D.; Lee, Y. H. Recent development of two-dimensional transition metal dichalcogenides and their applications. *Mater. Today* **2017**, *20*, 116−130.

(12) Kou, L.; Du, A.; Chen, C.; Frauenheim, T. Strain engineering of selective chemical adsorption on monolayer MoS_2. *Nanoscale* **2014**, *6*, 5156−5161.

(13) He, Q.; Zeng, Z.; Yin, Z.; Li, H.; Wu, S.; Huang, X.; Zhang, H. Fabrication of Flexible MoS_2 Thin-Film Transistor Arrays for Practical Gas-Sensing Applications. *Small* **2012**, *8*, 2994−2999.

(14) Yang, S.; Li, Y.; Wang, X.; Huo, N.; Xia, J. B.; Li, S. S.; Li, J. High performance few-layer GaS photodetector and its unique photo-response in different gas environments. *Nanoscale* **2014**, *6*, 2582−2587.

(15) Yang, S.; Yue, Q.; Cai, H.; Wu, K.; Jiang, C.; Tongay, S. Highly efficient gas molecule-tunable few-layer GaSe phototransistors. *J. Mater. Chem. C* **2016**, *4*, 248−253.

(16) Ou, J. Z.; Ge, W.; Carey, B.; Daeneke, T.; Rotbart, A.; Shan, W.; Wang, Y.; Fu, Z.; Chrimes, A. F.; Wlodarski, W.; Russo, S. P.; Li, Y. X.; Kalantar-zadeh, K. Physisorption-Based Charge Transfer in Two-Dimensional SnS_2 for Selective and Reversible NO_2 Gas Sensing. *ACS Nano* **2015**, *9*, 10313−10323.

(17) Liu, L.; Yang, Q.; Wang, Z.; Ye, H.; Chen, X.; Fan, X.; Zhang, G. High Selective Gas Detection for small molecules based on Germanium selenide monolayer. *Appl. Surf. Sci.* **2018**, *433*, 575−581.

(18) Yang, S.; Jiang, C.; Wei, S. H. Gas sensing in 2D materials. *Appl. Phys. Rev.* **2017**, *4*, No. 021304.

(19) Vargas-Bernal, R. Electrical Properties of Two-Dimensional Materials Used in Gas Sensors. *Sensors* **2019**, *19*, 1295.

(20) Liu, N.; Zhou, S. Gas adsorption on monolayer blue phosphorus: implications for environmental stability and gas sensors. *Nanotechnology* **2017**, *28*, 175708.

(21) Tang, X.; Du, A. J.; Kou, L. Z. Gas sensing and capturing based on two-dimensional layered materials: Overview from theoretical perspective. *WIREs Comput. Mol. Sci.* **2018**, *8*, No. e1361.

(22) Lei, J. C.; Zhang, X.; Zhou, Z. Recent advances in MXene: Preparation, properties, and applications. *Front. Phys.* **2015**, *10*, 276−286.

(23) Hong Ng, V. M.; Huang, H.; Zhou, K.; Lee, P. S.; Que, W.; Xu, J. Z.; Kong, L. B. Recent progress in layered transition metal carbides and/or nitrides (MXenes) and their composites: synthesis and applications. *J. Mater. Chem. A* **2017**, *5*, 3039−3068.

(24) Anasori, B.; Lukatskaya, M. R.; Gogotsi, Y. 2D metal carbides and nitrides (MXenes) for energy storage. *Nat. Rev. Mater.* **2017**, *2*, 16098.

(25) Zhang, H.; Yang, G.; Zuo, X.; Tang, H.; Yang, Q.; Li, G. Computational studies on the structural, electronic and optical properties of graphene-like MXenes (M_2CT_2, M=Ti, Zr, Hf; T=O, F, OH) and their potential applications as visible-light driven photocatalysts. *J. Mater. Chem. A* **2016**, *4*, 12913−12920.

(26) Lee, Y.; Cho, S. B.; Chung, Y. C. Tunable Indirect to Direct Band Gap Transition of Monolayer Sc_2CO_2 by the Strain Effect. *ACS Appl. Mater. Interfaces* **2014**, *6*, 14724−14728.

(27) Lee, Y.; Hwang, Y.; Cho, S. B.; Chung, Y. C. Achieving a direct band gap in oxygen functionalized-monolayer scandium carbide by applying an electric field. *Phys. Chem. Chem. Phys.* **2014**, *16*, 26273−26278.

(28) Naguib, M.; Come, J.; Dyatkin, B.; Presser, V.; Taberna, P. L.; Simon, P.; Barsoum, M. W.; Gogotsi, Y. MXene: a promising transition metal carbide anode for lithium-ion batteries. *Electrochem. Commun.* **2012**, *16*, 61−64.

(29) Sun, D.; Wang, M.; Li, Z.; Fan, G.; Fan, L. Z.; Zhou, A. Two-dimensional Ti_3C_2 as anode material for Li-ion batteries. *Electrochem. Commun.* **2014**, *47*, 80−83.

(30) Tang, Q.; Zhou, Z.; Shen, P. Are MXenes Promising Anode Materials for Li Ion Batteries? Computational Studies on Electronic Properties and Li Storage Capability of Ti_3C_2 and $Ti_3C_2X_2$ (X = F, OH) Monolayer. *J. Am. Chem. Soc.* **2012**, *134*, 16909−16916.

(31) Mashtalir, O.; Naguib, M.; Mochalin, V. N.; Dall'Agnese, Y.; Heon, M.; Barsoum, M. W.; Gogotsi, Y. Intercalation and delamination of layered carbides and carbonitrides. *Nat. Commun.* **2013**, *4*, 1716.

(32) Xie, Y.; Naguib, M.; Mochalin, V. N.; Barsoum, M. W.; Gogotsi, Y.; Yu, X.; Nam, K.-W.; Yang, X.-Q.; Kolesnikov, A. I.; Kent, P. R. C. Role of Surface Structure on Li-Ion Energy Storage Capacity of Two-Dimensional Transition-Metal Carbides. *J. Am. Chem. Soc.* **2014**, *136*, 6385−6394.

(33) Li, H.; Hou, Y.; Wang, F.; Lohe, M. R.; Zhuang, X.; Niu, L.; Feng, X. Flexible All-Solid-State Supercapacitors with High Volumetric Capacitances Boosted by Solution Processable MXene and Electrochemically Exfoliated Graphene. *Adv. Energy Mater.* **2017**, *7*, 1601847.

(34) Ghidiu, M.; Lukatskaya, M. R.; Zhao, M.-Q.; Gogotsi, Y.; Barsoum, M. W. Conductive two-dimensional titanium carbide 'clay' with high volumetric capacitance. *Nature* **2014**, *516*, 78−81.

(35) Lukatskaya, M. R.; Mashtalir, O.; Ren, C. E.; Dall'Agnese, Y.; Rozier, P.; Taberna, P. L.; Naguib, M.; Simon, P.; Barsoum, M. W.; Gogotsi, Y. Cation Intercalation and High Volumetric Capacitance of Two-Dimensional Titanium Carbide. *Science* **2013**, *341*, 1502.

(36) Liang, X.; Garsuch, A.; Nazar, L. F. Sulfur Cathodes Based on Conductive MXene Nanosheets for High-Performance Lithium−Sulfur Batteries. *Angew. Chem., Int. Edit.* **2015**, *54*, 3907−3911.

(37) Eames, C.; Islam, M. S. Ion Intercalation into Two-Dimensional Transition-Metal Carbides: Global Screening for New High-Capacity Battery Materials. *J. Am. Chem. Soc.* **2014**, *136*, 16270−16276.

(38) Er, D.; Li, J.; Naguib, M.; Gogotsi, Y.; Shenoy, V. B. Ti_3C_2 MXene as a High Capacity Electrode Material for Metal (Li, Na, K, Ca) Ion Batteries. *ACS Appl. Mater. Interfaces* **2014**, *6*, 11173−11179.

(39) Xie, Y.; Dall'Agnese, Y.; Naguib, M.; Gogotsi, Y.; Barsoum, M. W.; Zhuang, H. L.; Kent, P. R. C. Prediction and Characterization of MXene Nanosheet Anodes for Non-Lithium-Ion Batteries. *ACS Nano* **2014**, *8*, 9606−9615.

(40) Hu, T.; Zhang, H.; Wang, J.; Li, Z.; Hu, M.; Tan, J.; Hou, P.; Li, F.; Wang, X. Anisotropic electronic conduction in stacked two-dimensional titanium carbide. *Sci. Rep.* **2015**, *5*, 16329.

(41) Lipatov, A.; Alhabeb, M.; Lukatskaya, M. R.; Boson, A.; Gogotsi, Y.; Sinitskii, A. Effect of Synthesis on Quality, Electronic Properties and Environmental Stability of Individual Monolayer Ti_3C_2 MXene Flakes. *Adv. Electron. Mater.* **2016**, *2*, 1600255.

(42) Aïssa, B.; Ali, A.; Mahmoud, K. A.; Haddad, T.; Nedil, M. Transport properties of a highly conductive 2D $Ti_3C_2T_x$ MXene/graphene composite. *Appl. Phys. Lett.* **2016**, *109*, No. 043109.

(43) Hantanasirisakul, K.; Zhao, M.-Q.; Urbankowski, P.; Halim, J.; Anasori, B.; Kota, S.; Ren, C. E.; Barsoum, M. W.; Gogotsi, Y. Fabrication of $Ti_3C_2T_x$ MXene Transparent Thin Films with Tunable Optoelectronic Properties. *Adv. Electron. Mater.* **2016**, *2*, 1600050.

(44) Halim, J.; Lukatskaya, M. R.; Cook, K. M.; Lu, J.; Smith, C. R.; Näslund, L. Å.; May, S. J.; Hultman, L.; Gogotsi, Y.; Eklund, P.; Barsoum, M. W. Transparent Conductive Two-Dimensional Titanium Carbide Epitaxial Thin Films. *Chem. Mater.* **2014**, *26*, 2374−2381.

(45) Ma, T. Y.; Cao, J. L.; Jaroniec, M.; Qiao, S. Z. Interacting Carbon Nitride and Titanium Carbide Nanosheets for High-Performance Oxygen Evolution. *Angew. Chem., Int. Edit.* **2016**, *55*, 1138−1142.

(46) Seh, Z. W.; Fredrickson, K. D.; Anasori, B.; Kibsgaard, J.; Strickler, A. L.; Lukatskaya, M. R.; Gogotsi, Y.; Jaramillo, T. F.; Vojvodic, A. Two-Dimensional Molybdenum Carbide (MXene) as an Efficient Electrocatalyst for Hydrogen Evolution. *ACS Energy Lett.* **2016**, *1*, 589−594.

(47) Yang, X.; Gao, N.; Zhou, S.; Zhao, J. MXene nanoribbons as electrocatalysts for the hydrogen evolution reaction with fast kinetics. *Phys. Chem. Chem. Phys.* **2018**, *20*, 19390−19397.

(48) Junkaew, A.; Arróyave, R. Enhancement of the selectivity of MXenes (M_2C, M = Ti, V, Nb, Mo) via oxygen-functionalization: promising materials for gas-sensing and separation. *Phys. Chem. Chem. Phys.* **2018**, *20*, 6073−6082.

(49) Yu, X. F.; Li, Y. C.; Cheng, J. B.; Liu, Z. B.; Li, Q. Z.; Li, W. Z.; Yang, X.; Xiao, B. Monolayer Ti_2CO_2: A Promising Candidate for NH_3 Sensor or Capturer with High Sensitivity and Selectivity. *ACS Appl. Mater. Interfaces* **2015**, *7*, 13707−13713.

(50) Xiao, B.; Li, Y. C.; Yu, X. F.; Cheng, J. B. MXenes: Reusable materials for NH_3 sensor or capturer by controlling the charge injection. *Sens. Actuators B* **2016**, *235*, 103−109.

(51) Ma, S.; Yuan, D.; Jiao, Z.; Wang, T.; Dai, X. Monolayer Sc_2CO_2: A Promising Candidate as a SO_2 Gas Sensor or Capturer. *J. Phys. Chem. C* **2017**, *121*, 24077−24084.

(52) Ding, L.; Wei, Y.; Li, L.; Zhang, T.; Wang, H.; Xue, J.; Ding, L.-X.; Wang, S.; Caro, J.; Gogotsi, Y. MXene molecular sieving membranes for highly efficient gas separation. *Nat. Commun.* **2018**, *9*, 155.

(53) Chen, W. Y.; Jiang, X.; Lai, S.-N.; Peroulis, D.; Stanciu, L. Nanohybrids of a MXene and transition metal dichalcogenide for selective detection of volatile organic compounds. *Nat. Commun.* **2020**, *11*, 1302.

(54) Kresse, G.; Furthmüller, J. Efficient iterative schemes for ab initio total-energy calculations using a plane-wave basis set. *Phys. Rev. B* **1996**, *54*, 11169−11186.

(55) Perdew, J. P.; Burke, K.; Ernzerhof, M. Generalized Gradient Approximation Made Simple. *Phys. Rev. Lett.* **1996**, *77*, 3865−3868.

(56) Kresse, G.; Joubert, D. From ultrasoft pseudopotentials to the projector augmented-wave method. *Phys. Rev. B* **1999**, *59*, 1758−1775.

(57) Grimme, S.; Antony, J.; Ehrlich, S.; Krieg, H. A consistent and accurate ab initio parametrization of density functional dispersion correction (DFT-D) for the 94 elements H-Pu. *J. Chem. Phys.* **2010**, *132*, 154104.

(58) Caffrey, N. M.; Armiento, R.; Yakimova, R.; Abrikosov, I. A. Changes in work function due to NO_2 adsorption on monolayer and bilayer epitaxial graphene on SiC(0001). *Phys. Rev. B* **2016**, *94*, 205411.

(59) He, K.; Poole, C.; Mak, K. F.; Shan, J. Experimental demonstration of continuous electronic structure tuning via strain in atomically thin MoS_2. *Nano Lett.* **2013**, *13*, 2931−2936.

(60) Pérez Garza, H. H.; Kievit, E. W.; Schneider, G. F.; Staufer, U. Controlled, reversible, and nondestructive generation of uniaxial extreme strains (>10%) in graphene. *Nano Lett.* **2014**, *14*, 4107−4113.

(61) Ahn, G. H.; Amani, M.; Rasool, H.; Lien, D.-H.; Mastandrea, J. P.; Ager, J. W., III; Dubey, M.; Chrzan, D. C.; Minor, A. M.; Javey, A. Strain-engineered growth of two-dimensional materials. *Nat. Commun.* **2017**, *8*, 608.

(62) Ding, F.; Ji, H.; Chen, Y.; Herklotz, A.; Dörr, K.; Mei, Y.; Rastelli, A.; Schmidt, O. C. Stretchable graphene: a close look at fundamental parameters through biaxial straining. *Nano Lett.* **2010**, *10*, 3453−3458.

(63) King, A.; Johnson, G.; Engelberg, D.; Ludwing, W.; Marrow, J. Observations of Intergranular Stress Corrosion Cracking in a Grain-Mapped Polycrystal. *Science* **2008**, *321*, 382−385.

(64) Wiesner, M. R.; Lowry, G. V.; Casman, E.; Bertsch, P. M.; Mastson, C. W.; Giulio, R. T. D.; Liu, J.; Hochella, M. F. Meditations on the ubiquity and mutability of nano-sized materials in the environment. *ACS Nano* **2011**, *5*, 9703−9709.

(65) Wang, Y.; Li, F.; Li, Y.; Chen, Z. Semi-metallic Be_5C_2 monolayer global minimum with quasi-planar pentacoordinate carbons and negative Poisson's ratio. *Nat. Commun.* **2016**, *7*, 11488.

(66) Falin, A.; Cai, Q.; Santos, E. J. G.; Scullion, D.; Qian, D.; Zhang, Z.; Yang, Z.; Huang, S.; Watanabe, K.; Taniguch, T.; Barnett, M. R.; Chen, Y.; Rouff, R. S.; Li, L. H. Mechanical properties of atomically thin boron nitride and the role of interlayer interactions. *Nat. Commun.* **2017**, *8*, 15815.

(67) Young, A. F.; Dean, C. R.; Meric, I.; Sorgenfrei, S.; Ren, H.; Watanabe, K.; Taniguchi, T.; Hone, J.; Shepard, K. L.; Kim, P. Electronic compressibility of layer-polarized bilayer graphene. *Phys. Rev. B* **2012**, *85*, 235458.

(68) Fang, N.; Otsuka, K.; Ishii, A.; Taniguchi, T.; Watanabe, K.; Nagashio, K.; Kato, Y. K. Hexagonal boron nitride as an ideal substrate for carbon nanotube photonics. *ACS Photonics* **2020**, *7*, 1773−1779.